LETTERS
PUBLISHED ONLINE: 21 AUGUST 2011 | DOI: 10.1038/NNANO.2011.139
nature nanotechnology

Solution-processed core–shell nanowires for efficient photovoltaic cells

Jinyao Tang[1,3†], Ziyang Huo[1,3†], Sarah Brittman[1,3], Hanwei Gao[1,3] and Peidong Yang[1,2,3*]

Semiconductor nanowires are promising for photovoltaic applications[1–11], but, so far, nanowire-based solar cells have had lower efficiencies than planar cells made from the same materials[6–10,12,13], even allowing for the generally lower light absorption of nanowires. It is not clear, therefore, if the benefits of the nanowire structure, including better charge collection and transport[14] and the possibility of enhanced absorption through light trapping[4,15], can outweigh the reductions in performance caused by recombination at the surface of the nanowires and at p–n junctions. Here, we fabricate core–shell nanowire solar cells with open-circuit voltage and fill factor values superior to those reported for equivalent planar cells, and an energy conversion efficiency of ~5.4%, which is comparable to that of equivalent planar cells despite low light absorption levels[16]. The device is made using a low-temperature solution-based cation exchange reaction[17–21] that creates a heteroepitaxial junction between a single-crystalline CdS core and single-crystalline Cu_2S shell. We integrate multiple cells on single nanowires in both series and parallel configurations for high output voltages and currents, respectively. The ability to produce efficient nanowire-based solar cells with a solution-based process and Earth-abundant elements[22–24] could significantly reduce fabrication costs relative to existing high-temperature bulk material approaches.

Nanowire photovoltaics (PV) has been the subject of research with a view to enhancing the energy conversion efficiency and reducing the material and fabrication costs compared with bulk and thin-film PV. The core–shell geometry of nanowires is thought to be able to enhance the efficiency of charge collection by shortening the paths travelled by minority carriers[6,7,14]. However, nanowire solar cells demonstrate fill factors (FFs) and open-circuit voltages far inferior to those of their planar counterparts, suggesting lower charge collection efficiencies[6–8]. Possible reasons for this poor performance of nanowire solar cells include surface recombination and poor control over the quality of the material junction at the nanometre scale when high-temperature doping processes are used. On the other hand, heterojunction nanowire solar cells[11] containing suitably abrupt p–n junctions usually include a polycrystalline shell, which is associated with a high density of surface states, interface states and grain boundaries, which all reduce the efficiency of charge collection.

An ideal epitaxial core–shell configuration is highly desirable for its low recombination rate and high collection efficiency; however, the high fabrication costs associated with gas-phase epitaxial chemical vapour deposition (CVD)[25] or molecular beam epitaxy (MBE)[12] prevent its widespread application. The solution-based cation exchange reaction, on the other hand, provides a facile, low-cost method to prepare high-quality heteroepitaxial nanomaterials[17–20]. Furthermore, the cation exchange reaction circumvents the difficulties of high-temperature doping and deposition for nanomaterials, which suggests much lower fabrication costs and better reproducibility.

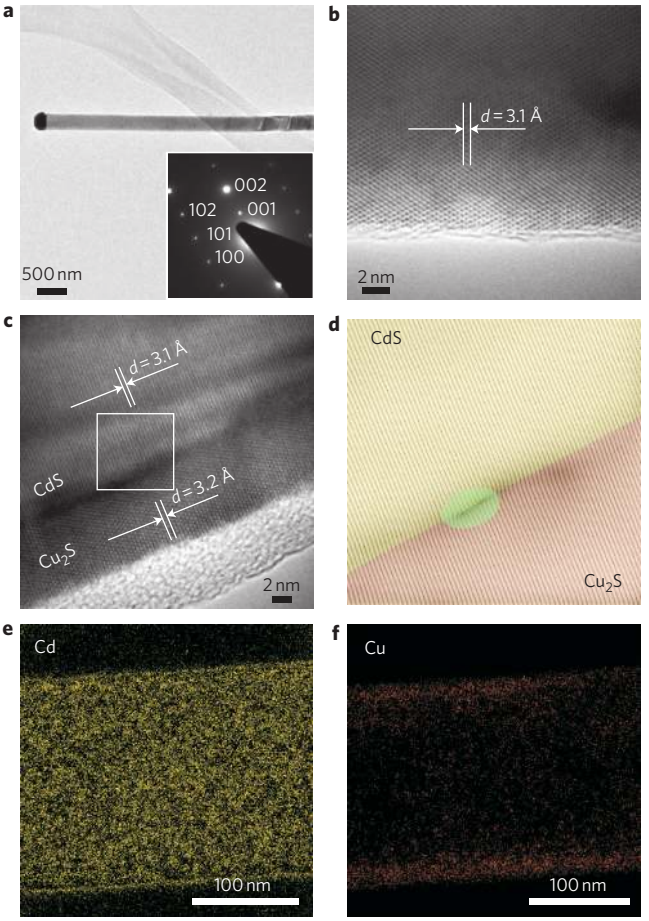

Figure 1 | Structural characterization of CdS and CdS–Cu_2S core–shell nanowires. a, Representative TEM image of an as-grown CdS nanowire with its tip capped by a gold nanoparticle. Inset: electron diffraction pattern taken on the single crystalline nanowire. **b**, High-resolution TEM image of an individual CdS nanowire, showing the single crystalline structure. **c**, High-resolution TEM image of a CdS–Cu_2S nanowire at the heterojunction. **d**, Constructed inverse FFT image along the growth direction for the area marked in **c**. The green area shows the typical lattice fringe distortion at the core–shell interface (see Supplementary Information). **e**–**f**, EELS elemental mapping images for Cd (**e**) and Cu (**f**), respectively.

The core–shell nanowires were prepared using a solution-based cation exchange reaction. The initial CdS nanowires were synthesized

[1]Department of Chemistry, University of California, Berkeley, California 94720, USA, [2]Department of Materials Science and Engineering, University of California, Berkeley, California 94720, USA, [3]Materials Sciences Division, Lawrence Berkeley National Laboratory, Berkeley, California 94720, USA; [†]These authors contributed equally to this work. *e-mail: p_yang@berkeley.edu

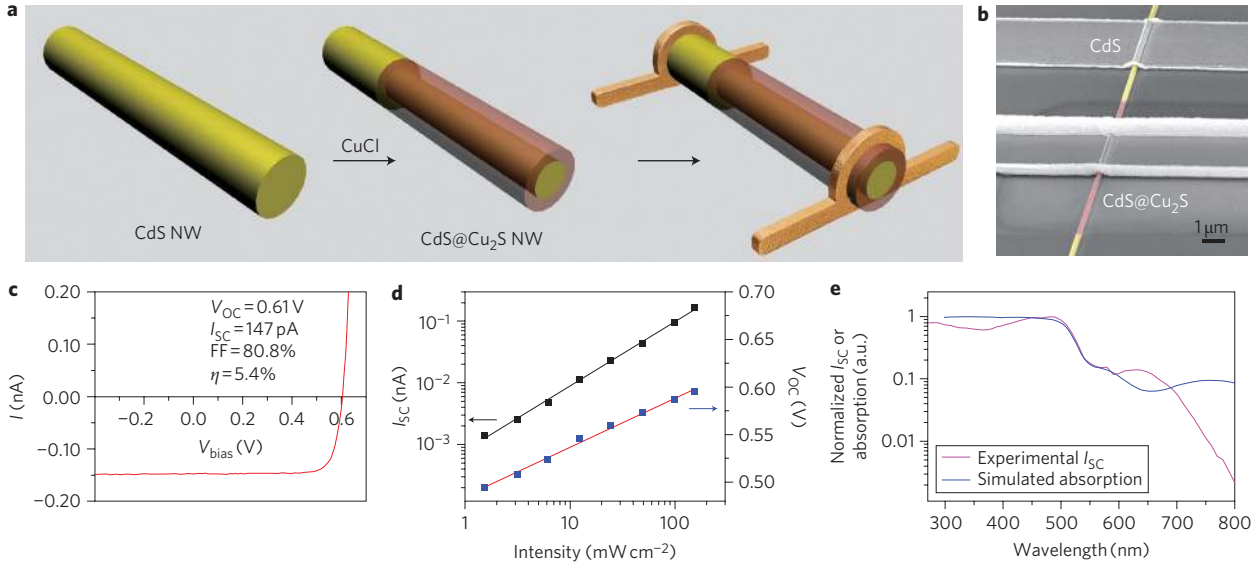

Figure 2 | Fabrication and characterization of CdS–Cu_2S core–shell nanowire PV devices. a, Schematic of the fabrication process. From left to right, a CdS (yellow) nanowire (NW) is partially converted in CuCl solution to form a layer of Cu_2S (brown) shell, then metal contacts were deposited on the CdS core and Cu_2S shell. The Al_2O_3 masking step is not shown. **b**, SEM image of a PV unit; CdS and Cu_2S are highlighted with yellow and brown false colours, respectively. **c**, *I*–*V* characteristic of a core–shell nanowire under 1 sun (AM 1.5G) illumination. **d**, Light intensity dependence of the photocurrent (I_{SC}) and open-circuit voltage (V_{OC}). **e**, Wavelength dependence of the photocurrent compared with simulated nanowire absorption. Photocurrent (red curve) was normalized by the photon flux of the source and matches well the absorption spectrum of the simulated CdS–Cu_2S core–shell nanowire with similar dimensions (blue curve).

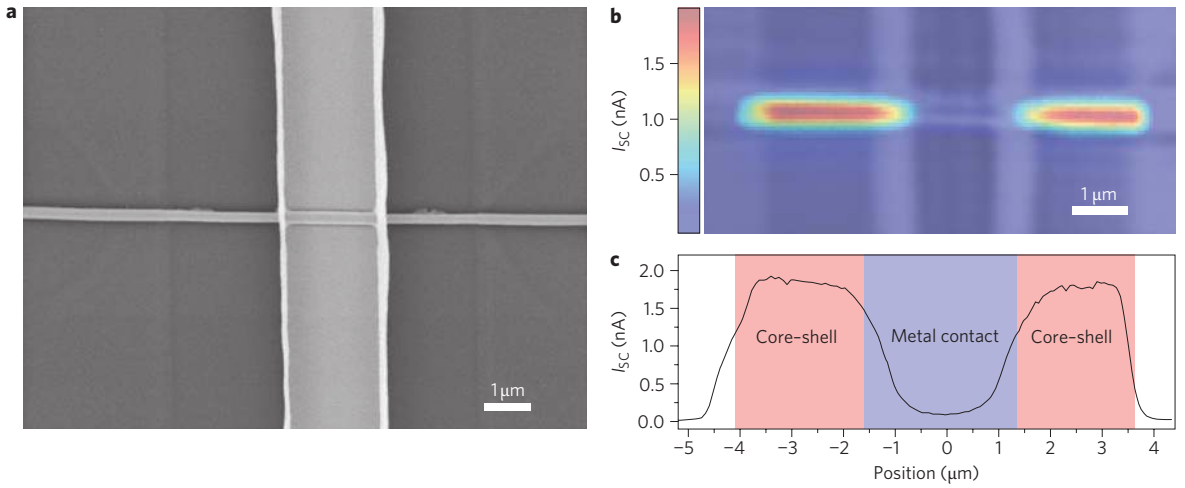

Figure 3 | SPCM of a core–shell nanowire. a, SEM image of the PV device with metal contact shown in b. **b**, SPCM image superimposed on the confocal reflection image collected simultaneously shows that only the core–shell portion of the nanowire is active for solar energy conversion. **c**, Line profile of the photocurrent along the nanowire, revealing uniform photocurrent in the core–shell region.

by physical vapour transport using a vapour–liquid–solid (VLS) mechanism[26] rather than wet chemistry[27], thereby achieving material of better quality and with greater physical length. The as-grown single-crystalline CdS nanowires have diameters of between 100 and 400 nm and lengths up to 50 μm, as shown in scanning electron microscopy (SEM) images (see Supplementary Information). The morphology of the CdS nanowires was further confirmed by transmission electron microscopy (TEM; Fig. 1a). Figure 1b shows the single-crystalline hexagonal crystal phase of the CdS nanowire, which is consistent with results from powder X-ray diffraction (see Supplementary Information). The spacing of the lattice fringes measured from Fig. 1b is ~3.1 Å, which corresponds to the (101) plane of wurtzite CdS and is consistent with the electron diffraction pattern (Fig. 1a, inset).

The as-grown CdS nanowire was dipped into a 0.5 M CuCl solution at 50 °C for 5–10 s to convert the surface CdS to a Cu_2S shell. From the TEM image (Fig. 1c), the single-crystalline Cu_2S shell was measured to be 5–20 nm thick, and its thickness could be controlled by the reaction time (see Supplementary Information). The spacing of the lattice fringes in the shell is ~3.2 Å, which corresponds to the (222) plane of low-chalcocite Cu_2S. Along the oriented direction, the lattice mismatch is less than 4%, allowing epitaxial growth with minimal formation of structural defects. In Fig. 1d, the selected inverse fast Fourier transform (FFT) image shows that most of the lattice fringes are smooth and continuous across the junction, and that less than 10% distortion exists at the heterostructure interface in the marked area. Furthermore, the *in situ* electron energy loss spectrum

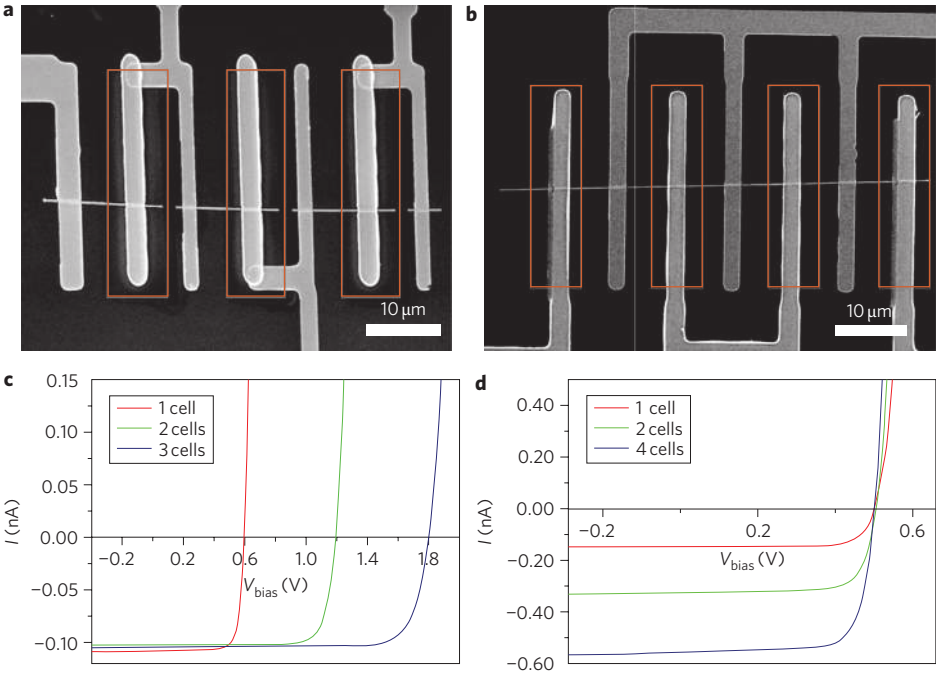

Figure 4 | Multiple PV units on a single nanowire, in series and in parallel. a, SEM image of three PV units from a single nanowire in series with the core–shell regions marked by the brown rectangles. **b**, SEM image of four PV units from a single nanowire in parallel with the core–shell regions marked by the brown rectangles. **c**, *I*–*V* characteristic of the in series units under 1 sun illumination (AM 1.5G), showing that the voltages add and the current remains fixed. **d**, *I*–*V* characteristic of the four units in parallel under 1 sun illumination (AM 1.5G), showing that the currents add and the voltage remains fixed.

(EELS) mapping in Fig. 1e,f shows that cadmium is uniformly dispersed throughout the nanowire, whereas copper is concentrated near the surface, confirming the core–shell structure.

To characterize the PV performance of the CdS–Cu_2S nanowires, devices were fabricated as illustrated in Fig. 2a. Briefly, the CdS nanowire was masked with Al_2O_3, and then the mask was removed with buffered hydrofluoric acid (BHF) in a region defined by photolithography. After cation exchange in the CuCl solution, metal electrodes were deposited for ohmic contact (Fig. 2b). As the CdS nanowire was intrinsic, and therefore highly resistive (>1 TΩ) in the dark, the dark current was below our measurement sensitivity (~0.1 pA) in the measurement region (–1 V to 1 V). Under 1 sun illumination (AM 1.5G), the photogenerated carriers dramatically reduced the resistivity of the CdS to ~0.1 GΩ, which is negligible in the current measurement (voltage drop of ~0.01 V for the short-circuit condition).

Figure 2c shows the *I*–*V* characteristic of these core–shell nanowire devices, clearly demonstrating the advantages of the heteroepitaxial junction PV device. The device shows high-quality diode behaviour, with an ideality factor of $n \approx 1.2$, a large open-circuit voltage V_{OC} of up to 0.61 V, and an excellent FF of over 80%. Even though the Cu_2S thin-film solar cell has been researched for over four decades, this nanowire device exhibits by far the best recorded V_{OC} and FF, which are close to their theoretical limits[28] (the maximum V_{OC} and FF values reported for thin-film Cu_2S–CdS solar cells are ~540 mV and 71%[28,29]). Because these two values are directly related to the junction quality and carrier recombination, we attribute these improvements to the virtues of both the heteroepitaxial junction and the high carrier collection efficiency of the core–shell nanowire structure. Furthermore, the devices are relatively stable under ambient and illuminated operation conditions (see Supplementary Information). These nanowire PV cells also exhibit a high parallel resistance R_P, over 1 TΩ, implying less degradation in performance under low illumination conditions, such as those present in indoor applications. As shown in Fig. 2d, the V_{OC} drops more slowly with decreasing light intensity ($\Delta V_{OC}/\Delta \ln(I) = 22.5$ mV) than in a silicon nanowire[6] ($\Delta V_{OC}/\Delta \ln(I) \approx 56$ mV) or in Cu_2S thin-film PVs[30] ($\Delta V_{OC}/\Delta \ln(I) \approx 39$ mV). Compared with previously reported silicon and GaAs nanowire solar cells[6,7], the main advantage of our system is the abrupt and epitaxial interface between its p- and n-type materials. Because the ratio of junction area to absorption material volume in a nanowire solar cell is significantly larger than the same ratio in a bulk solar cell, a nearly epitaxial interface with low defect density is key to achieving improved charge collection while minimizing carrier recombination at the interface.

Our nanowire PV cells were ~4.95 μm long and 260 nm in diameter, and yielded a short-circuit current I_{SC} of 147 pA. Because the nanowire PV active area is confined to its lithographically defined core–shell region, as confirmed by scanning photocurrent mapping (SPCM, Fig. 3), we estimated the active area as its geometric cross-section (1.29 μm^2) and calculated an upper limit to the current density as 11.4 mA cm^{-2} and the corresponding conversion efficiency as ~5.4%. The wavelength dependence of the photocurrent (Fig. 2e) shows that much less photocurrent is generated at wavelengths longer than 520 nm, where only Cu_2S can absorb. This is mainly because the thickness of the Cu_2S shell (5–20 nm) allows it to absorb only 10–20% of the available longer-wavelength photons, as confirmed by a numerically simulated absorption spectrum (Fig. 2e). We have also observed a drop in current density for core–shell nanowires with thinner shells, suggesting that the energy conversion efficiency of this new core–shell nanowire cell can be further improved by increasing the thickness of the Cu_2S shell within the structure.

SPCM was performed to examine the active area in the PV device[7,8]. As shown in Fig. 3, the active area is confined to the lithographically defined cation-exchange conversion region, which confirms that the core–shell nanowire does indeed generate all the measured photocurrent. Two plateaux appear in the photocurrent line profile along the length of the nanowire (Fig. 3c). This

indication of uniform charge collection along the core–shell nanowire confirms the low series resistance loss of the CdS core and Cu_2S shell. Furthermore, the sharp decrease in current at the edge of the core–shell region implies a short minority carrier diffusion length ($L < 1$ μm) within the CdS. For such a material, it is expected that the solar cell will benefit from the improved collection efficiency of the core–shell nanowire structure over that of a planar thin film[14].

We further demonstrated the reproducibility and versatility of our nanowire PV cells by constructing multiple units on a single nanowire in either parallel or series configurations. As is shown in Fig. 4, three cells in series and four cells in parallel were prepared on a single CdS nanowire. In each case, high V_{OC} or high I_{SC} were obtained without a decrease in the FF (~80%). When individual solar cells are connected for higher output power, it is important that the cells in parallel have matching voltages and the cells in series have matching currents to maximize the performance of the module. Because our PV units were built on the same nanowire, superior uniformity of I_{SC}, V_{OC} and FF between units can be readily achieved, resulting in virtually no power loss after the connection of individual cells.

In summary, we have presented a method to prepare CdS–Cu_2S core–shell nanowires using a solution-based cation exchange reaction. Advantages of this solution-based method include its simplicity and potential low cost, as well as its use of Earth-abundant elements. Furthermore, the heterojunction prepared by this method is atomically well defined with few interface defects, enabling excellent charge separation with minimal minority carrier recombination. As a result, our nanowire PV device shows excellent V_{OC}, FF and response to low light levels compared with both planar solar cells and to previously reported nanowire solar cells. At present, the efficiency of our CdS–Cu_2S devices is limited mainly by their light absorption, which can probably be improved by using a thicker Cu_2S shell or by taking advantage of the light-trapping effects found in nanowire arrays. We expect that creating a similarly high-quality interface within silicon or group III–V nanowire-based solar cells will also improve the energy conversion efficiency of these devices. Our demonstration of excellent V_{oc} and FF within a core–shell nanowire shows that, by creating such high-quality interfaces, nanowire-based solar cells can achieve a charge collection superior to that of their planar counterparts. This achievement, together with the increased light absorption already demonstrated in nanowires, indicates that core–shell nanowires are truly promising components for future PV devices.

Methods

CdS nanowire synthesis. Growth of CdS nanowires was carried out in a 1-inch quartz tube furnace. CdS powder (99.999%, Alfa Aesar) was loaded into the centre of the tube as the source. A 10 nm gold thin film was deposited on a silicon substrate as a catalyst for one-dimensional growth. Growth was carried out at 800 °C with ~100–200 s.c.c.m. argon as a carrier gas for ~30 min.

Device fabrication. After growth, the CdS nanowires were dispersed in isopropanol (IPA) and drop-cast onto a silicon substrate with 200 nm thermal oxide. The silicon substrate loaded with CdS nanowires was then coated with 20 nm Al_2O_3 by atomic layer deposition at 200 °C. For units in series, nanowires were cut into several 15-μm-long segments by photolithography followed by etching in HCl vapour. The conversion area was also defined photolithographically, and the Al_2O_3 mask was removed by dipping into 1:10 buffered hydrofluoric acid (BHF) for 30 s. Cation conversion was performed by dipping the substrate into 0.5 M CuCl solution at 50 °C for 5–10 s. The substrate was then thoroughly rinsed with deionized water, acetone and IPA and blown dry with nitrogen. Metal contacts to the CdS and Cu_2S were defined by photolithography and electron-beam evaporation of indium/gold (5 nm/100 nm) and platinum/gold (10 nm/90 nm), respectively, at ~2×10^{-6} torr. No annealing was required to obtain ohmic contact.

Optical and electrical measurements. A 150 W xenon arc lamp (Newport Corporation) with an AM 1.5G filter was used to characterize the PV device response, and the light intensity was calibrated using a NREL calibrated silicon photodiode. *I–V* characterization was performed with a Keithley 236 source-measure unit (SMU). The parallel resistance of the device was calculated by taking the derivative of the *I–V* curve in the short-circuit condition. A home-built confocal microscope with piezoelectric scanning stage was used for simultaneous reflection imaging and SPCM. A helium–cadmium laser ($\lambda = 442$ nm) was focused to a diffraction-limited spot through the objective lens of the microscope (NA = 0.95), with a power density of ~10–15 W cm^{-2}. At each point in the reflection imaging, the photocurrent was recorded by the Keithley SMU. The image resolution for both measurements was 128 × 64 pixels. Photocurrent maps were plotted using MATLAB[31], and the reflection images were processed using *Image SXM*[32]. The dependence of the photocurrent on wavelength (Fig. 2e) was obtained by measuring the photocurrent generated in the device at 10 nm increments, normalized by the photon flux of the source. A 300 W xenon arc lamp (Newport Corporation) was coupled to a monochromator (Newport Corporation) to obtain monochromatic illumination. The output of the source was measured using a calibrated photodiode (Newport Corporation).

Nanowire absorption spectrum simulation. The optical absorption spectrum was calculated using finite-difference time-domain methods (Lumerical FDTD Solutions 7.0). A nanowire with a 230-nm-diameter CdS core and 10-nm-thick Cu_2S shell was considered in the model. An orthogonal meshing size of 2 nm was used in the nanowire region, which was proven fine enough by a convergence test. The optical absorption of the nanowire was obtained by monitoring the power flow in and out of a monitor box enclosing the nanowire.

Received 22 June 2011; accepted 18 July 2011;
published online 21 August 2011

References

1. Huynh, W. U., Dittmer, J. J. & Alivisatos, A. P. Hybrid nanorod–polymer solar cells. *Science* **295,** 2425–2427 (2002).
2. Gur, I., Fromer, N. A., Geier, M. L. & Alivisatos, A. P. Air-stable all-inorganic nanocrystal solar cells processed from solution. *Science* **310,** 462–465 (2005).
3. Wu, Y. *et al.* Synthesis and photovoltaic application of copper(I) sulfide nanocrystals. *Nano Lett.* **8,** 2551–2555 (2008).
4. Garnett, E. & Yang, P. Light trapping in silicon nanowire solar cells. *Nano Lett.* **10,** 1082–1087 (2010).
5. Law, M. *et al.* Nanowire dye-sensitized solar cells. *Nature Mater.* **4,** 455–459 (2005).
6. Tian, B. *et al.* Coaxial silicon nanowires as solar cells and nanoelectronic power sources. *Nature* **449,** 885–889 (2007).
7. Czaban, J. A., Thompson, D. A. & LaPierre, R. R. GaAs core–shell nanowires for photovoltaic applications. *Nano Lett.* **9,** 148–154 (2008).
8. Kelzenberg, M. D. *et al.* Photovoltaic measurements in single-nanowire silicon solar cells. *Nano Lett.* **8,** 710–714 (2008).
9. Kempa, T. J. *et al.* Single and tandem axial p-i-n nanowire photovoltaic devices. *Nano Lett.* **8,** 3456–3460 (2008).
10. Dong, Y., Tian, B., Kempa, T. J. & Lieber, C. M. Coaxial group III-nitride nanowire photovoltaics. *Nano Lett.* **9,** 2183–2187 (2009).
11. Fan, Z. *et al.* Three-dimensional nanopillar-array photovoltaics on low-cost and flexible substrates. *Nature Mater.* **8,** 648–653 (2009).
12. Goto, H. *et al.* Growth of core–shell InP nanowires for photovoltaic application by selective-area metal organic vapor phase epitaxy. *Appl. Phys. Express* **2,** 035004 (2009).
13. Wei, W. *et al.* Direct heteroepitaxy of vertical InAs nanowires on Si substrates for broad band photovoltaics and photodetection. *Nano Lett.* **9,** 2926–2934 (2009).
14. Kayes, B. M., Atwater, H. A. & Lewis, N. S. Comparison of the device physics principles of planar and radial p–n junction nanorod solar cells. *J. Appl. Phys.* **97,** 114302 (2005).
15. Cao, L. *et al.* Resonant germanium nanoantenna photodetectors. *Nano Lett.* **10,** 1229–1233 (2010).
16. Martinuzzi, S. Trends and problems in cadmium sulfide (CdS)/copper sulfide (CuxS) thin film solar cells: a review. *Sol. Cells* **5,** 243–268 (1982).
17. Son, D. H., Hughes, S. M., Yin, Y. & Paul Alivisatos, A. Cation exchange reactions in ionic nanocrystals. *Science* **306,** 1009–1012 (2004).
18. Robinson, R. D. *et al.* Spontaneous superlattice formation in nanorods through partial cation exchange. *Science* **317,** 355–358 (2007).
19. Luther, J. M., Zheng, H., Sadtler, B. & Alivisatos, A. P. Synthesis of PbS nanorods and other ionic nanocrystals of complex morphology by sequential cation exchange reactions. *J. Am. Chem. Soc.* **131,** 16851–16857 (2009).
20. Sadtler, B. *et al.* Selective facet reactivity during cation exchange in cadmium sulfide nanorods. *J. Am. Chem. Soc.* **131,** 5285–5293 (2009).
21. Jain, P. K., Amirav, L., Aloni, S. & Alivisatos, A. P. Nanoheterostructure cation exchange: anionic framework conservation. *J. Am. Chem. Soc.* **132,** 9997–9999 (2010).
22. Trentler, T. J. *et al.* Solution–liquid–solid growth of crystalline III–V semiconductors: an analogy to vapor–liquid–solid growth. *Science* **270,** 1791–1794 (1995).
23. Ouyang, L. *et al.* Catalyst-assisted solution–liquid–solid synthesis of CdS/CdSe nanorod heterostructures. *J. Am. Chem. Soc.* **129,** 133–138 (2006).

24. Dong, A., Wang, F., Daulton, T. L. & Buhro, W. E. Solution–liquid–solid (SLS) growth of ZnSe–ZnTe quantum wires having axial heterojunctions. *Nano Lett.* **7,** 1308–1313 (2007).
25. Lauhon, L. J., Gudiksen, M. S., Wang, D. & Lieber, C. M. Epitaxial core–shell and core–multishell nanowire heterostructures. *Nature* **420,** 57–61 (2002).
26. Duan, X. F. & Lieber, C. M. General synthesis of compound semiconductor nanowires. *Adv. Mater.* **12,** 298–302 (2000).
27. Li, Y. D. *et al.* Nonaqueous synthesis of CdS nanorod semiconductor. *Chem. Mater.* **10,** 2301–2303 (1998).
28. Bragagnolo, J. A. *et al.* The design and fabrication of thin-film cadmium sulfide/copper(I) sulfide cells of 9.15% conversion efficiency. *IEEE Trans. Electron. Dev.* **ED-27,** 645–651 (1980).
29. Rothwarf, A. & Barnett, A. M. Design analysis of thin-film CdS–Cu_2S solar-cell. *IEEE Trans. Electron. Dev.* **24,** 381–387 (1977).
30. Bryant, F. J. & Glew, R. W. Analysis of the current–voltage characteristics of cadmium sulphide solar cells under varying light intensities. *Ener. Convers.* **14,** 129–133 (1975).
31. MATLAB version R2008b (MathWorks Inc., 2008).
32. Barrett, S. D. Image SXM http://www.ImageSXM.org.uk (2008).

Acknowledgements

This work was supported by the Director, Office of Science, Office of Basic Energy Sciences, Materials Sciences and Engineering Division, of the US Department of Energy (contract no. DE-AC02-05CH11231). The work on devices integrated in parallel and in series was supported by the National Science Foundation (NSF, contract no. 0832819). The authors thank the National Center for Electron Microscopy for use of their facilities.

Author contributions

J.T., Z.H. and P.Y. conceived and designed the experiments. J.T. fabricated the devices and performed the measurements. Z.H. collected and analysed the TEM images. S.B. was responsible for the scanning photocurrent mapping. H.G. provided the simulation results. J.T., Z.H. and P.Y. co-wrote the paper. All authors discussed the results and revised the manuscript.

Additional information

The authors declare no competing financial interests. Supplementary information accompanies this paper at www.nature.com/naturenanotechnology. Reprints and permission information is available online at http://www.nature.com/reprints. Correspondence and requests for materials should be addressed to P.Y.